iScience

CellPress
OPEN ACCESS

Article

MRPL12-ANT3 interaction involves in acute kidney injury via regulating MPTP of tubular epithelial cells

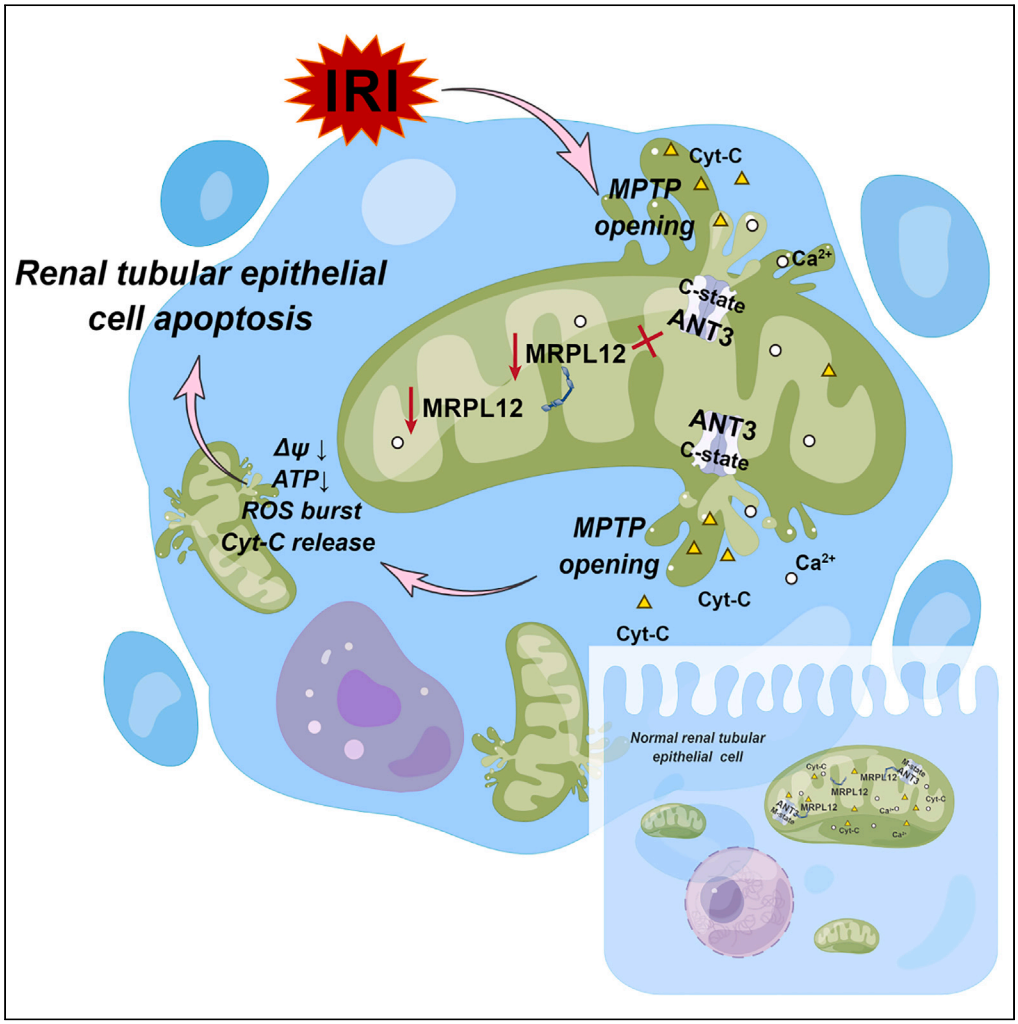

Xingzhao Ji, Lingju Chu, Dun Su, ..., Qian Mu, Yi Liu, Qiang Wan

liuyishanyi@email.sdu.edu.cn (Y.L.)
wanqiang@sdu.edu.cn (Q.W.)

Highlights

MRPL12 interacts with ANT3 specifically

MRPL12 manipulates MPTP via influencing ANT3 conformation

MRPL12-ANT3 interaction involves in acute kidney injury via regulating MPTP

Ji et al., iScience 26, 106656
May 19, 2023
https://doi.org/10.1016/j.isci.2023.106656

iScience

CellPress
OPEN ACCESS

Article

MRPL12-ANT3 interaction involves in acute kidney injury via regulating MPTP of tubular epithelial cells

Xingzhao Ji,[1,2,4,5,7] Lingju Chu,[1,6,7] Dun Su,[1,6,7] Jian Sun,[2,4,5] Peng Song,[2,4,5] Shengnan Sun,[1,6] Ying Wang,[2,4,5] Qian Mu,[2,4,5] Yi Liu,[2,3,4,5,*] and Qiang Wan[1,6,8,*]

SUMMARY

Acute kidney injury (AKI) is a serious disease with no effective treatment. Abnormal opening of mitochondrial permeability transition pore (MPTP) is an important pathological process in ischemia reperfusion injury (IRI), the key factor of AKI. It is essential to elucidate MPTP regulation mechanism. Here, we identified mitochondrial ribosomal protein L7/L12 (MRPL12) specifically binds to adenosine nucleotide translocase 3 (ANT3) under normal physiological conditions, stabilizes MPTP and maintains mitochondrial membrane homeostasis in renal tubular epithelial cells (TECs). During AKI, MRPL12 expression was significantly decreased in TECs, and MRPL12-ANT3 interaction was reduced, leading to ANT3 conformation change, MPTP abnormal opening, and cell apoptosis. Importantly, MRPL12 overexpression protected TECs from MPTP abnormal opening and apoptosis during hypoxia/reoxygenation (H/R). Our results suggest MRPL12-ANT3 axis involves in AKI by regulating MPTP, and MRPL12 could be potential intervention target for treatment of AKI.

INTRODUCTION

Acute kidney injury (AKI) has been recognized as a major public health problem affecting millions of patients worldwide and leads to decreased survival.[1] In view of the increasing morbidity and mortality of AKI and the consequent financial burden, effective treatment is urgently needed. However, there has been no effective intervention other than supportive therapy in improving AKI thus far.[2] A leading cause of AKI is ischemia reperfusion injury (IRI), which results from compromised perfusion to renal tissue.[3] It has been determined that pathophysiological abnormalities of IRI are characterized by tubular injury and cell death, tissue inflammation, and changes in renal hemodynamics.[3]

Mitochondria are essential regulators of cellular energy metabolism, especially in metabolically active organs. Kidneys are organs with a high energy demand, and renal tubules are densely packed with mitochondria.[4,5] The homeostasis of renal tubular epithelial cells heavily relies on normal mitochondrial function. Emerging evidence supports the idea that damaged mitochondria with disrupted matrix cristae and mitochondrial permeability-mediated programmed cell death (PCD) are crucial to ischemic AKI.[6,7]

Mitochondrial permeability transition pore (MPTP) opening has been proposed as the key driver of ischemia/reperfusion (I/R) injury.[8] MPTP is a mitochondrial inner membrane channel that opens in response to a variety of cellular damage factors and acute elevations in matrix Ca^{2+} concentration.[9] Opening of the MPTP allows solutes of up to 1.5 kDa to freely diffuse across the inner mitochondrial membrane.[9] MPTP opening also causes the mitochondrial H^+ gradient to dissipate, which uncouples the mitochondria and collapses the mitochondrial membrane potential.[9] This energetic catastrophe with mitochondrial swelling and rupture initiates programmed cell death.[9]

At present, adenosine nucleotide translocase (ANT), cyclophilin D (CypD), phosphate carrier (PiC), F_1F_0 ATP synthase and Bax/Bak have been suggested to form the MPTP complex.[10] Humans possess four ANT genes that have similar structures and high sequence homology.[11] ANT1 (*SLC25A4*) is the predominant isoform in terminally differentiated, metabolically active tissues.[12,13] ANT2 (*SLC25A5*) is expressed in many tissues but is enriched in proliferating cell types.[12,14] ANT3 (*SLC25A6*) is expressed in virtually all

[1]Center of Cell Metabolism and Disease, Central Hospital Affiliated to Shandong First Medical University, Jinan, Shandong 250021, China

[2]Department of Pulmonary and Critical Care Medicine, Shandong Provincial Hospital Affiliated to Shandong First Medical University, Jinan, Shandong 250021, China

[3]Department of Pulmonary and Critical Care Medicine, Shandong Provincial Hospital, Shandong University, Jinan, Shandong 250021, China

[4]Shandong Key Laboratory of Infections Respiratory Disease, Jinan, Shandong 250021, China

[5]Medical Science and Technology Innovation Center, Shandong First Medical University & Shandong Academy of Medical Sciences, Jinan, Shandong 250021, China

[6]Key Laboratory of Cell Metabolism in Medical and Health of Shandong Provincial Health Commission, Central Hospital Affiliated to Shandong First Medical University, Jinan, Shandong 250021, China

[7]These authors contributed equally

[8]Lead contact

*Correspondence: liuyishanyi@email.sdu.edu.cn (Y.L.), wanqiang@sdu.edu.cn (Q.W.)

https://doi.org/10.1016/j.isci.2023.106656

tissues.[12,15] ANT4 (*SLC25A31*) is expressed in the human brain, liver, and testis.[16] ANT interconverts between a mitochondrial matrix facing m-state conformation and intermembrane space (IMS) facing c-state conformation during ADP/ATP exchange.[17–19] The m-state cannot transition directly into the MPTP pore; however, the c-state can.[9,18] Any drug that stabilizes the conformation of ANT in which it faces the cytosol (the c-state) enhances MPTP opening, whereas stabilization of ANT in the matrix (the m-state) inhibits MPTP opening.[8,20–22]

The opening of MPTP is related to the conformational change in ANT. The m-state of ANT inhibits MPTP opening, whereas the c-state of ANT promotes MPTP opening. ANT conformation research has been highly informed by two unique classes of ANT inhibitors.[18] The first is atractyloside (ATR), a potent inhibitor of ATP/ADP transfer that binds ANT proteins in the nucleotide binding site, reversibly locking ANT proteins in the c-state. Notably, this inhibition can be overcome via competition with ADP, which drives ANT proteins back into the m-state. The second ANT inhibitor, bongkrekic acid (BKA), is another potent inhibitor of ATP/ADP exchange. In contrast to ATR, BKA can be used to lock ANT proteins in the m-state conformation. The differential targeting of these two inhibitors has proven invaluable in determining the kinetic and structural features of ANT proteins.[9]

Opening of the MPTP represents a major therapeutic target, as it can be mitigated by a number of compounds interacting with its pore-forming components. However, the regulatory mechanism of MPTP opening in renal tubular epithelial cells in AKI has not been fully elucidated.[23]

Mitochondrial ribosomes, as vital components of mitochondria, have also been intensively investigated because of their involvement in human pathologies,[24] including cardiomyopathies and developmental abnormalities,[25,26] cancer,[27] and hearing loss.[28] Mitochondrial ribosomal protein L7/L12 (MRPL12) is an important mitochondrial ribosomal protein discovered in recent years. In addition to influencing mitochondrial translation by binding to the mitochondrial ribosome subunit, MRPL12 can also exist in a ribosome-free form within mitochondria and directly bind to mitochondrial RNA polymerase (POLRMT), promoting mtDNA transcription.[29,30] In brief, MRPL12 is involved in the regulation of oxidative phosphorylation (OXPHOS) and mitochondrial energy metabolism at both the transcriptional and translational levels. Thus, MRPL12 is a multifunctional mitochondrial ribosomal protein. Recently, we found that MRPL12 was significantly downregulated in AKI.[31,32] However, whether MRPL12 is involved in other important cellular processes in AKI in addition to OXPHOS has not been clarified. In this study, we identified a novel mechanism whereby MRPL12 ameliorates MPTP opening by interacting with ANT3, contributing to the protection of renal tubular epithelial cells from apoptosis and the maintenance of kidney homeostasis during renal IRI. Our findings therefore point to a vital role for the MRPL12-ANT3 axis in protecting renal tubular epithelial cells from AKI. Moreover, MRPL12 could serve as a potential intervention target for the treatment of AKI.

RESULTS

MRPL12 interacts with ANT3 specifically

Previously, we found that the expression of MRPL12 was decreased during AKI. To further study the potential role of MRPL12 during AKI, we performed immunoprecipitation assays on HK-2 cell lysates using anti-MRPL12 IgG or isotype control IgG, followed by mass spectrometry, to identify proteins which interact with MRPL12. Fourteen proteins were specifically present in the anti-MRPL12 IgG pull-down samples compared with the isotype control IgG pull-down samples. Surprisingly, ANT3, the pore-forming protein of MPTP, was found to be enriched in the anti-MRPL12 IgG pull-down samples compared with the isotype control IgG pull-down samples (Figure 1A).

To further verify the interaction of MRPL12 and ANT3, we first performed a proximity ligation assay in HK-2 cells. As shown in (Figures 1B and 1C), MRPL12 specifically binds to ANT3 but not to ANT1/2 (ANT1/2/3 are recognized to have similar structures and high sequence homology). In addition, an endogenous protein coimmunoprecipitation assay showed that MRPL12 could specifically interact with ANT3 but not with ANT1/2 (Figures 1D and 1E). To further demonstrate the specificity of ANT3 binding to MRPL12, a proximity ligation assay and endogenous protein coimmunoprecipitation confirmed that ANT3 could not bind to MRPL11, a mitochondrial ribosomal protein most closely related to MRPL12[33] (Figures 1F and 1G). Moreover, molecular docking identified that proteins MRPL12 and ANT3 formed a stable protein docking model (Table S1 and Figure S1). Importantly, immunoelectron microscopy revealed that MRPL12 exists in the

A

Protein	Total score			
	Input(IgG)	Input(IP)	IgG	IP
EF-1	929084996	735944314	0	235682870
ANT3	**23898552**	**168128366**	**0**	**219366182**
RPL10	109774350	53204559.5	0	210683492
MRPL43	9197439	2569686	0	45300111
RPSA	191719120	202992892	0	20575761
TUFM	191113388	106342971	0	9074889
CSDE1	16483142.8	19273645.2	0	4102292
APMAP	16551297.5	18610859	0	3684141
DNAJA2	18147857.8	8402080.94	0	3223100
FAM50A	5978943	46475842.5	0	3033525
HSD17B4	38059338	35200844	0	2091084
AIFM1	17817214.8	6877327.19	0	1828247
HSP1A	218561479	153778237	0	1585702
PPP1CA	42167558.5	8330373.25	0	1168027

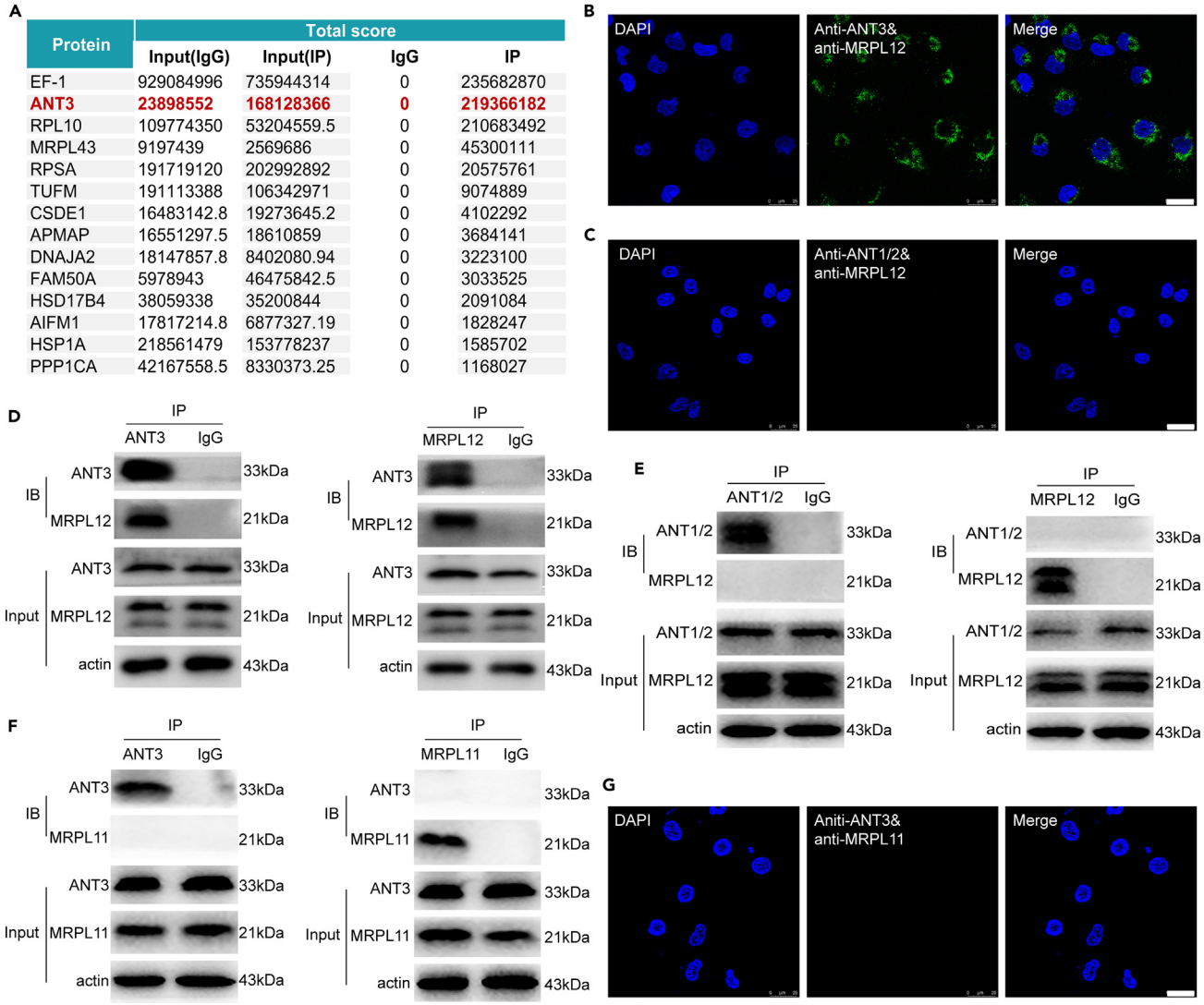

Figure 1. MRPL12 interacts with ANT3 specifically

(A) Mass spectrometry assay. The criteria for identifying candidate binding partners are described in the results. The total scores of candidate proteins were calculated by analysis software and are listed in descending order.

(B) Interaction of MRPL12 and ANT3 in HK-2 cells visualized by the Duolink@ proximity ligation assay. Scale bars = 25 μm.

(C) Duolink@ proximity ligation assay of MRPL12 and ANT1/2 in HK-2 cells. Scale bars = 25 μm.

(D) Coimmunoprecipitation assay of MRPL12 and ANT3 in HK-2 cells.

(E) Coimmunoprecipitation assay of MRPL12 and ANT1/2 in HK-2 cells.

(F) Coimmunoprecipitation assay of MRPL11 and ANT3 in HK-2 cells.

(G) Duolink@ proximity ligation assay of MRPL11 and ANT3 in HK-2 cells. Scale bars = 25 μm. The independent experiments above were performed in triplicate.

mitochondrial membrane (Figures S2A-S2D). The above results indicated that MRPL12 can interact with ANT3 specifically in renal tubular epithelial cells.

MRPL12 influences the opening of MPTP via ANT3

We then examined whether MRPL12 altered ANT3 expression in HK-2 cells. First, we constructed MRPL12 overexpression and knockdown cell lines. The mRNA and protein levels of ANT3 were analyzed after the knockdown and overexpression of MRPL12. As shown in (Figures 2A–2F), both overexpression and knockdown of MRPL12 had no effect on the expression of ANT3 at the mRNA or protein levels.

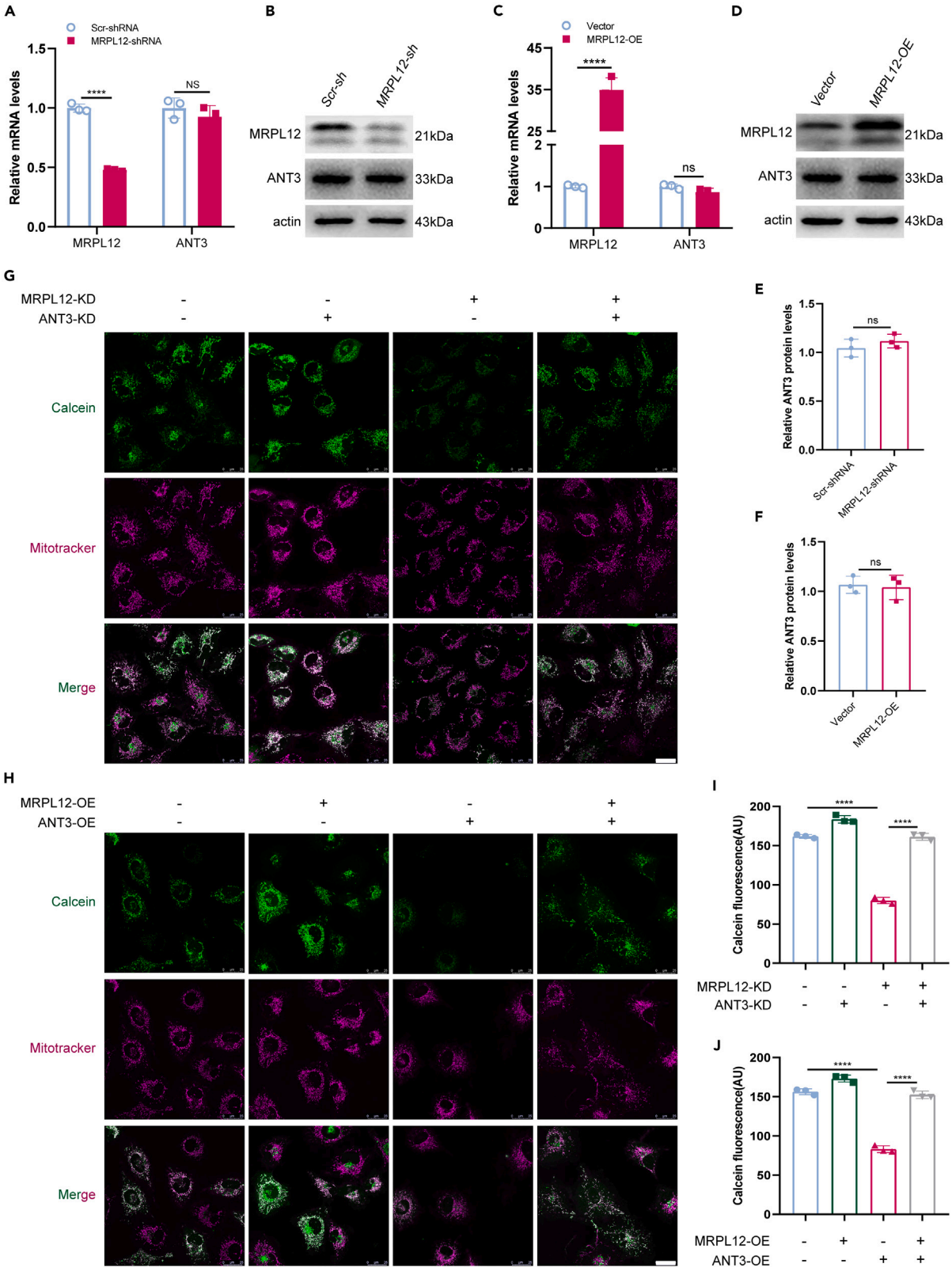
A
Scr-shRNA
MRPL12-shRNA
Relative mRNA levels
1.5
1.0
0.5
0.0
****
NS
MRPL12
ANT3
B
Scr-sh
MRPL12-sh
MRPL12
ANT3
actin
21kDa
33kDa
43kDa
C
Vector
MRPL12-OE
Relative mRNA levels
45
35
25
2
1
0
****
ns
MRPL12
ANT3
D
Vector
MRPL12-OE
MRPL12
ANT3
actin
21kDa
33kDa
43kDa
G
MRPL12-KD
ANT3-KD
Calcein
Mitotracker
Merge
E
Relative ANT3 protein levels
1.5
1.0
0.5
0.0
ns
Scr-shRNA
MRPL12-shRNA
F
Relative ANT3 protein levels
1.5
1.0
0.5
0.0
ns
Vector
MRPL12-OE
H
MRPL12-OE
ANT3-OE
Calcein
Mitotracker
Merge
I
Calcein fluorescence(AU)
200
150
100
50
0
****
****
MRPL12-KD
ANT3-KD
J
Calcein fluorescence(AU)
200
150
100
50
0
****
****
MRPL12-OE
ANT3-OE

Figure 2. MRPL12 influences the opening of MPTP via ANT3

(A–F) qRT−PCR and Western blotting were performed to detect MRPL12 and ANT3 expression in HK-2 cells transfected with MRPL12-silencing shRNA or MRPL12-overexpressing plasmids.

(G and H) The opening of the mPTP in HK-2 cells was detected by a $CoCl_2$-calcein fluorescence quenching assay. After $CoCl_2$ quenching, calcein fluorescence decreased, indicating MPTP pore opening. Scale bars = 25 μm.

(I and J) Quantification of calcein fluorescence was performed using Image J and is shown in the histogram. The independent experiments above were performed in triplicate. The differences were analyzed by Student's *t* test. Data are presented as the mean ± SD, ****p<0.0001.

We further explored whether the dysregulation of MRPL12 influenced MPTP. MRPL12 was overexpressed or knocked down in HK-2 cells, followed by a $CoCl_2$-calcein fluorescence quenching assay to assess the opening of the transient MPTP.[21,34] We found that MPTP opening increased after MRPL12 knockdown in HK-2 cells (Figures 2G–2I). In contrast, MPTP opening decreased after MRPL12 overexpression (Figures 2H–2J). In addition, transmission electron microscope analysis demonstrated typical changes of morphological damage of TECs mitochondria in TEC-MRPL12$^{-/-}$ mice, i.e., mitochondria swelling, rupture of the mitochondrial membrane and distorted mitochondrial cristae (disruption or loss) (Figures S3A and S3B).

Then, the role of ANT3 in the regulation of MRPL12-dependent MPTP was determined. qRT−PCR and western blotting showed the overexpression or knockdown efficiency of ANT3 in HK-2 cells (Figures S4A–S4D). We found that MPTP opening induced by MRPL12 knockdown was effectively reversed by ANT3 knockdown (Figures 2G–2I). Consistent with these conclusions, coexpression of ANT3 with MRPL12 completely abrogated the ability of MRPL12 to decrease MPTP opening (Figures 2H–2J). Taken together, these data demonstrated that the influence of MRPL12 on MPTP opening is ANT3-dependent.

MRPL12 manipulates MPTP opening by influencing ANT3 conformation

To further identify the specific region of MRPL12 bound to ANT3, plasmids with full-length (FL) MRPL12 and MRPL12 deletion mutants (DMs) were constructed. HEK293T cells were cotransfected with MRPL12 FL and DMs with HA labels and full-length ANT3 plasmids with FLAG labels (Figure 3A). Coimmunoprecipitation assays revealed that MRPL12 DM3 dramatically abolished the MRPL12-ANT3 interaction in 293T cells. However, truncation of other regions of MRPL12 did not affect the combination of MRPL12 and ANT3 (Figure 3B). These findings suggested that amino acids 91–128 are essential for the interaction between MRPL12 and ANT3.

To investigate whether MRPL12 manipulates MPTP opening by influencing ANT3 conformation, we next knocked down MRPL12 followed by the addition of 5 μM BKA in HK-2 cells and found that BKA treatment effectively reversed the increase in MPTP opening induced by MRPL12 knockdown (Figures 3C and 3D). In contrast, overexpression of MRPL12 was followed by the addition of 5 μM ATR in HK-2 cells, and the results indicate that ATR treatment reversed the decrease in MPTP opening caused by MRPL12 overexpression (Figures 3E and 3F). Moreover, MRPL12 DM3 overexpression was unable to significantly reverse ATR-induced MPTP opening (Figures 3E and 3F), which indicated that MRPL12 binds ANT3 via the 91–128 amino acid region of MRPL12 and affects the conformation of ANT3, thus affecting MPTP opening.

Indeed, MRPL12 is involved in the process of OXPHOS as a mitochondrial ribosomal protein.[30,32] Therefore, it is an open question whether MRPL12 influences MPTP opening by regulating OXPHOS or via ANT3. Of interest, as shown in (Figure 3G), MRPL12 DM3 overexpression also elevated the subunits of OXPHOS complex contents in HK-2 cells, similar to overexpression of MRPL12 (FL), which suggested that the function of MRPL12 DM3 in regulating mitochondrial OXPHOS was not significantly decreased. This evidence further corroborated that MRPL12 modulates MPTP opening by interacting with ANT3 and changing its conformation rather than by regulating OXPHOS. Taken together, these results demonstrated that the binding of MRPL12 with ANT3 specifically might promote the ANT3 m-state conformation and ameliorates MPTP opening.

MRPL12 involves in mitochondria-mediated apoptosis in an ANT3-dependent manner

The translocation of cytochrome *c* (cyt-C) from mitochondria to the cytosol because of MPTP opening was proven to be a crucial biomarker of mitochondrial-mediated apoptosis.[35] Therefore, the potential role of MRPL12 in mitochondrial-mediated apoptosis in HK-2 cells was investigated. First, we found that apoptosis

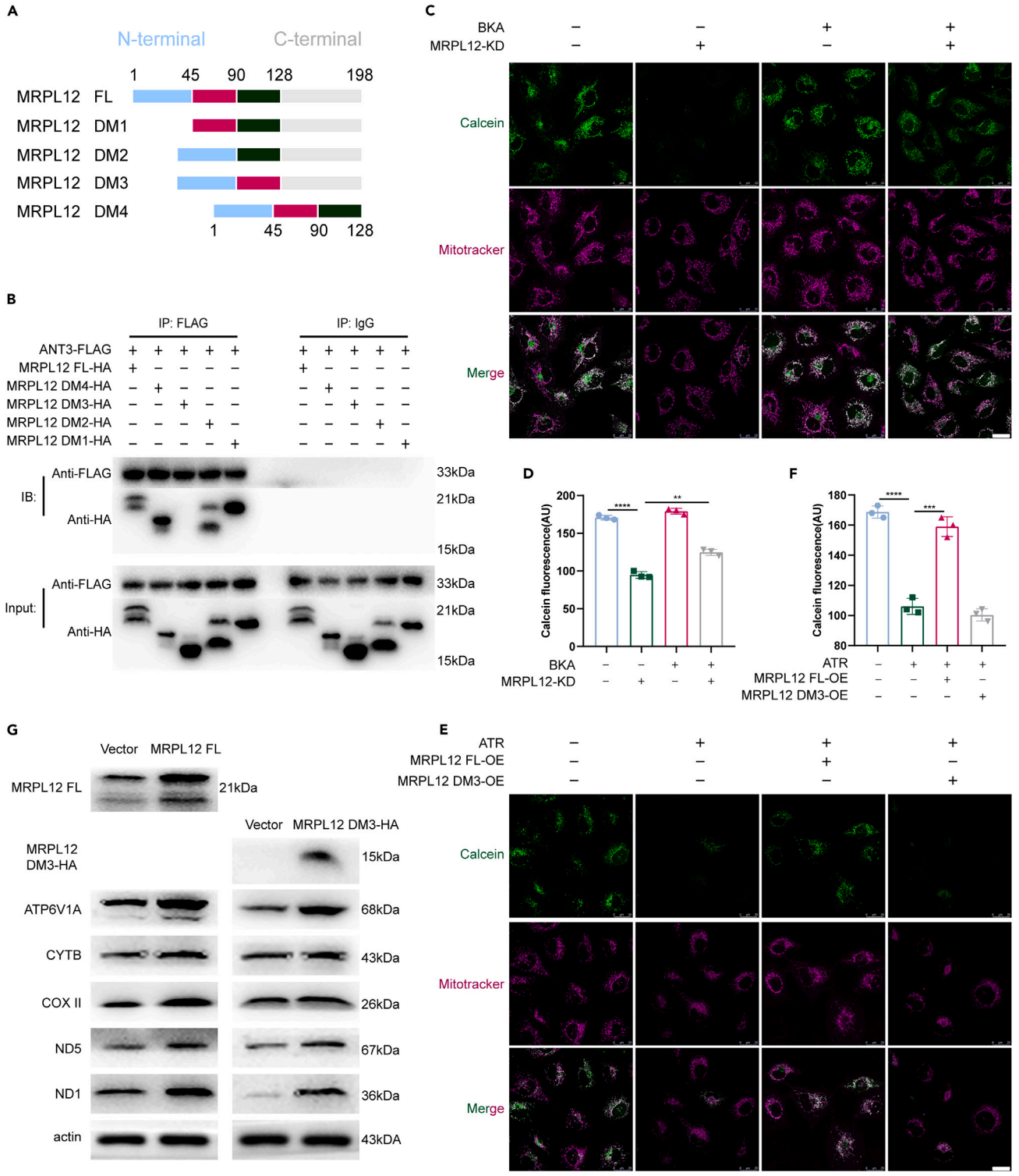

Figure 3. MRPL12 manipulates MPTP opening by influencing ANT3 conformation

(A) Domain structure of MRPL12 FL and MRPL12 DMs. MRPL12 DM1: 45–198 amino acids; MRPL12 DM2: 1–45 and 91–198 amino acids; MRPL12 DM3: 1–90 and 129–198 amino acids; MRPL12 DM4: 1–128 amino acids.

Figure 3. *Continued*

(B) FLAG and rabbit immunoglobulin (IgG, used as a negative control) immunoprecipitations (IP) of lysates from 293 T cells cotransfected with ANT3-FLAG and MRPL12 FL-HA or the indicated MRPL12 DMs-HA. Immunoprecipitates were immunoblotted (IB) either with HA or FLAG antibodies to examine deletion mutants of MRPL12 or ANT3, respectively.

(C and E) The opening of the MPTP in HK-2 cells was detected by a $CoCl_2$-calcein fluorescence quenching assay. After $CoCl_2$ quenching, calcein fluorescence decreased, indicating MPTP pore opening. Scale bars = 25 μm.

(D and F) Quantification of calcein fluorescence was calculated by Image J and is shown in the histogram.

(G) Western blotting for OXPHOS components in MRPL12 FL-overexpressing or MRPL12 DM3-overexpressing HK-2 cells. The independent experiments above were performed in triplicate. The differences were analyzed by Student's *t* test. Data are presented as the mean ± SD, **p<0.01, ***p<0.001 and ****p<0.0001.

of HK-2 cells increased after MRPL12 knockdown. Then, on MRPL12 knockdown, further ANT3 knockdown effectively alleviated HK-2 cell apoptosis (Figures 4A and 4B). In contrast, we found that overexpression of MRPL12 but not MRPL12 DM3 effectively alleviated HK-2 cell apoptosis induced by the addition of the ANT inhibitor ATR (Figures 4C and 4D). We further confirmed that apoptosis induced by MRPL12 downregulation was cyt-C related. As shown in (Figures 4E and 4F), increased cytosolic cyt-C levels as well as decreased mitochondrial cyt-C levels were revealed in MRPL12 knockdown HK-2 cells, indicating that MRPL12 knockdown promoted the release of a mitochondrial pro-apoptotic factor (cyt-C) to activate the apoptotic program. Notably, mitochondrial cyt-C release induced by MRPL12 knockdown was ameliorated by ANT3 knockdown (Figures 4E and 4F). Concomitantly, ATR-induced mitochondrial cyt-C release was improved by MRPL12 but not MRPL12 DM3 overexpression (Figures 4G and 4H). Collectively, these data indicated that MPTP activation (MPTP opening) induced by diminishing MRPL12 and ANT3 interactions promoted mitochondrial cyt-C release, which resulted in apoptosis in HK-2 cells.

The MRPL12/ANT3 interaction is diminished in I/R-injured kidneys and H/R-treated HK-2 cells

Furthermore, we investigated the role of MRPL12 in AKI. First, we constructed H/R model *in vitro* using HK-2 cells. We found that MRPL12 expression decreased in HK-2 cells subjected to H/R treatment, whereas ANT3 expression remained unchanged (Figures 5A–5C and 5E–5G). Importantly, coimmunoprecipitation assay confirmed that the interaction between MRPL12 and ANT3 was eliminated after H/R treatment (Figures 5A, 5D, 5E, and 5H). These results were further confirmed by proximity ligation assay (Figure 5I). The above indicated the MRPL12/ANT3 interaction is diminished as a consequence of MRPL12 decrease *in vitro* H/R model.

Then, renal IRI models were established in C57BL/6J mice. The right kidney was subjected to nephrectomy as internal control. The left renal artery was clamped for 30 min of warm ischemia at 37°C followed by 24 h of reperfusion. After I/R treatment, renal function analysis revealed that the levels of serum creatinine (sCr) and blood urea nitrogen (BUN) were significantly increased (Figures 5J and 5K). Furthermore, HE staining was used to better assess the area of injury and degree of damage to renal tubules. As shown in (Figure 5L), tubular dilation, vacuolar degeneration of tubular epithelial cells and loss of the tubular brush border were apparent in the renal cortex after I/R treatment. Moreover, the left kidney developed serious renal morphological injury and prominently high HE injury scores compared to the right kidney (Figure 5M). These results indicate that the IRI-induced AKI model was successfully established. Immunohistochemistry revealed that I/R treatment groups exhibited a significant reduction in MRPL12 in the renal cortex compared with control groups, whereas ANT3 expression was unchanged (Figures S5A and S5B). Similar findings were also observed in renal biopsies of patients with AKI (Figures 5N–5Q). Then, we further analyzed the interaction between MRPL12 and ANT3 under ischemia reperfusion conditions *in vivo*. The results of proximity ligation assay further corroborated that the interaction between MRPL12 and ANT3 was eliminated in the kidney tissue of both AKI patients (Figure 5R) and mice (Figure S5C). These results suggested that the MRPL12/ANT3 interaction is eliminated as a consequence of MRPL12 decrease *in vitro* and *in vivo* AKI models.

MRPL12 attenuates MPTP opening by interacting with ANT3 under H/R conditions

Because the above findings revealed that MRPL12 was downregulated and the interaction of MRPL12 and ANT3 was attenuated *in vitro* and *in vivo* AKI models, it is hypothesized that overexpression of MRPL12 might rescue the abnormal phenotype of HK-2 cells mediated by H/R treatments. First, western blotting showed the overexpression efficiency of MRPL12 in HK-2 cells under normal or H/R treatments (Figure S6). And as shown in (Figures 6A and 6B), MRPL12 overexpression indeed elevated the interaction of MRPL12 and ANT3 in H/R-treated HK-2 cells. Confocal microscopy analyses showed that MRPL12 overexpression effectively ameliorated

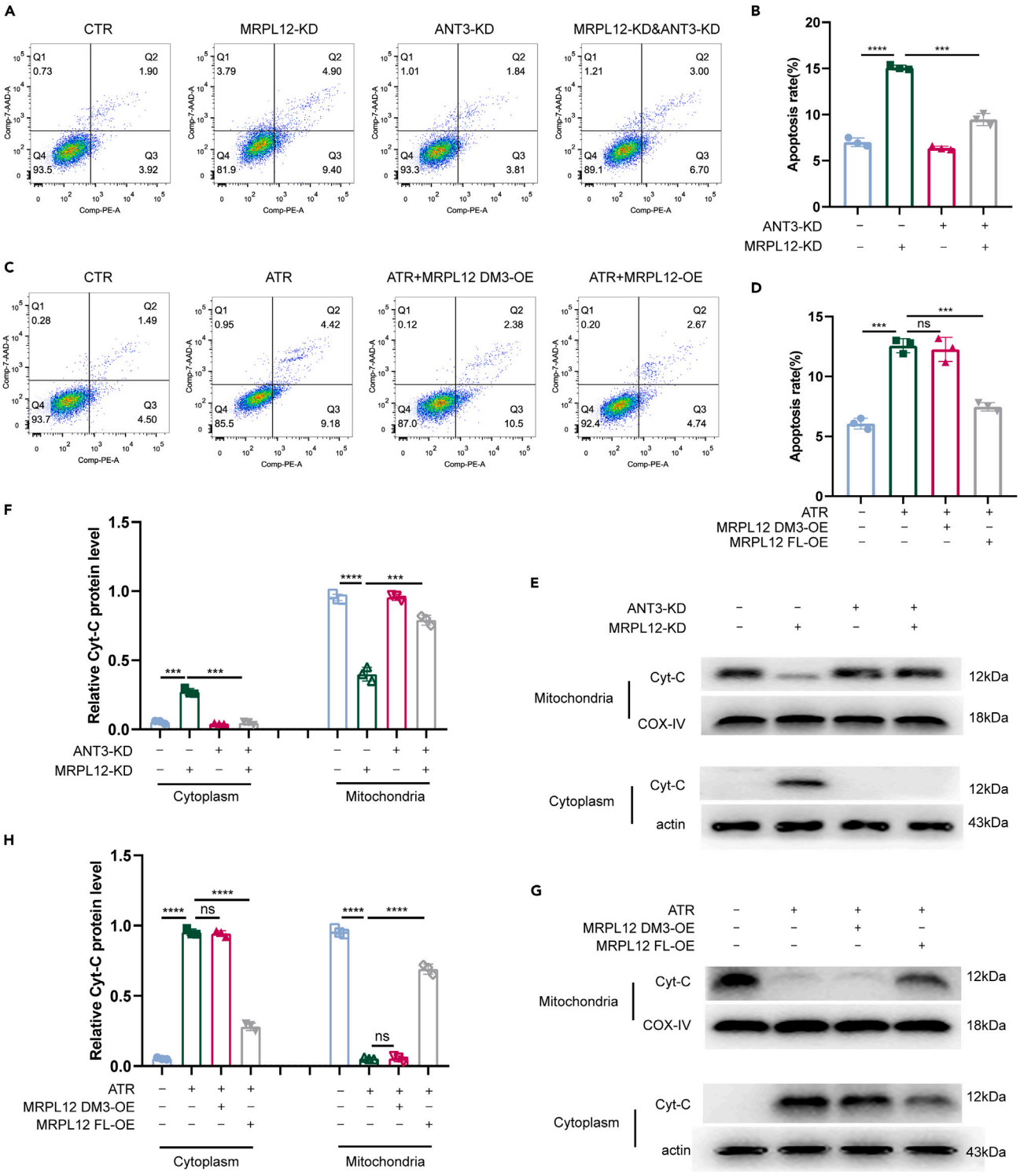

Figure 4. MRPL12 involves in mitochondria-mediated apoptosis in an ANT3-dependent manner

(A and B) Apoptosis in HK-2 cells was detected by flow cytometry analysis. The results of flow cytometry analysis were quantified.

(C and D) Apoptosis in HK-2 cells was detected by flow cytometry analysis. Cells transfected with MRPL12 FL-overexpressing plasmid or MRPL12 DM3-overexpressing plasmid were treated with 5 μM ATR. The results of flow cytometry analysis were quantified.

Figure 4. *Continued*

(E and F) Release of cyt-C from the mitochondria to the cytoplasm in HK-2 cells. Cells were fractionated into the cytoplasm and the mitochondria. Cyt-C protein levels were assessed by Western blot analysis.

(G and H) The release of cyt-C from the mitochondria to the cytoplasm in HK-2 cells was assessed by Western blot analysis. Cells transfected with MRPL12 FL-overexpressing plasmid or MRPL12 DM3-overexpressing plasmid were treated with 5 μM ATR. The independent experiments above were performed in triplicate. The differences were analyzed by Student's *t* test. Data are presented as the mean ± SD, ***p<0.001 and ****p<0.0001.

H/R-induced MPTP opening in HK-2 cells, but MRPL12 DM3 overexpression did not (Figures 6C and 6D). In contrast, knockdown of MRPL12 remarkably aggravated H/R-triggered MPTP opening in HK-2 cells (Figures 6E and 6F). These results indicated that H/R-induced MPTP opening is attenuated by MRPL12 upregulation and aggravated by MRPL12 downregulation, which is mediated to MRPL12/ANT3 interaction.

MRPL12 alleviates mitochondria-mediated apoptosis by interacting with ANT3 under H/R conditions

Based on the results above, we hypothesized that MRPL12 overexpression can protect against HK-2 cells apoptosis triggered by H/R. As shown in (Figures 7A and 7B), immunoblotting revealed that MRPL12 knockdown markedly aggravated cyt-C release from mitochondria to the cytosol induced by H/R in HK-2 cells. Flow cytometry analysis also showed that MRPL12 knockdown markedly promoted H/R-induced apoptosis in HK-2 cells (Figures 7C and 7D). Otherwise, MRPL12 overexpression dramatically mitigated cyt-C release in H/R-induced HK-2 cells (Figures 7E and 7F). Importantly, MRPL12 overexpression largely attenuated the H/R-mediated apoptosis of HK-2 cells (Figures 7G and 7H). These results indicated that downregulation of MRPL12 aggravates the mitochondria-related apoptosis of renal tubular epithelial cells induced by H/R. Importantly, upregulation of MRPL12 protects renal tubular epithelial cells from the mitochondria-related apoptosis induced by H/R.

DISCUSSION

The kidney is second only to the heart in mitochondrial count and oxygen consumption. As such, the health and status of the energy powerhouse, the mitochondria, is pivotal to the health and proper function of the kidney.[5] Renal tubular epithelial cell death caused by renal mitochondrial dysfunction is considered to be one of the most important pathways in the pathogenesis of AKI.[32] Hence, mitochondria are critical mediators of cellular life through energy production, as well as death through the induction of apoptosis and necrosis.[10]

Persistent MPTP opening has emerged as a final common pathway to cell death underlying many disease states.[23] Specific pharmacological modulation of MPTP opening has long been sought. Although the MPTP is clearly a druggable target, the development of inhibitors beyond the prototypical compound Cyclosporin A (CsA), itself limited by off-target effects and low therapeutic efficacy, has been slow and disappointing.[23] CsA inhibits the Ca^{2+}-activated phosphatase calcineurin, binds to the CypD component of the MPTP and inhibits MPTP opening.[36] However, CsA is intrinsically nephrotoxic and may promote tubular cell apoptosis, dedifferentiation, and an inflammatory response.[36] This limits its use as an agent protecting mitochondria in the setting of AKI. Therefore, it is imperative to explore other regulatory mechanisms for targeted intervention of MPTP in the treatment of AKI.

ANT was recognized as the inner membrane pore-forming component of the MPTP given that ATR and BKA, the latter being an ANT inhibitor that stabilizes the 'm' conformation of the protein, inhibits MPTP activity, whereas ATR, an ANT effector that promotes the 'c' conformation of the protein, stimulates MPTP opening.[10] Exploring the potential mechanisms for regulating MPTP opening through ANT might provide more effective strategies for interventions targeting MPTP.

The mammalian mitochondrial ribosome consists of associated large (39S) and small (28S) ribosomal subunits, with each subunit composed of tRNAs encoded by mtDNA and multiple mitochondrial ribosomal proteins (MRPs) encoded by nuclear DNA and imported into the mitochondrial matrix.[32] Recently, several MRPs have been implicated in multiple cellular processes, such as cell proliferation and cell cycle regulation, in addition to OXPHOS.[32] In the present study, we found that MRPL12 can effectively protect renal tubular epithelial cells from apoptosis in AKI by binding to ANT3 specifically.

Emerging data suggest that mammalian mitoribosomes synthesize 13 proteins, all of which are highly hydrophobic membrane protein components of the mitochondrial respiratory chain. Early experiments showed that some

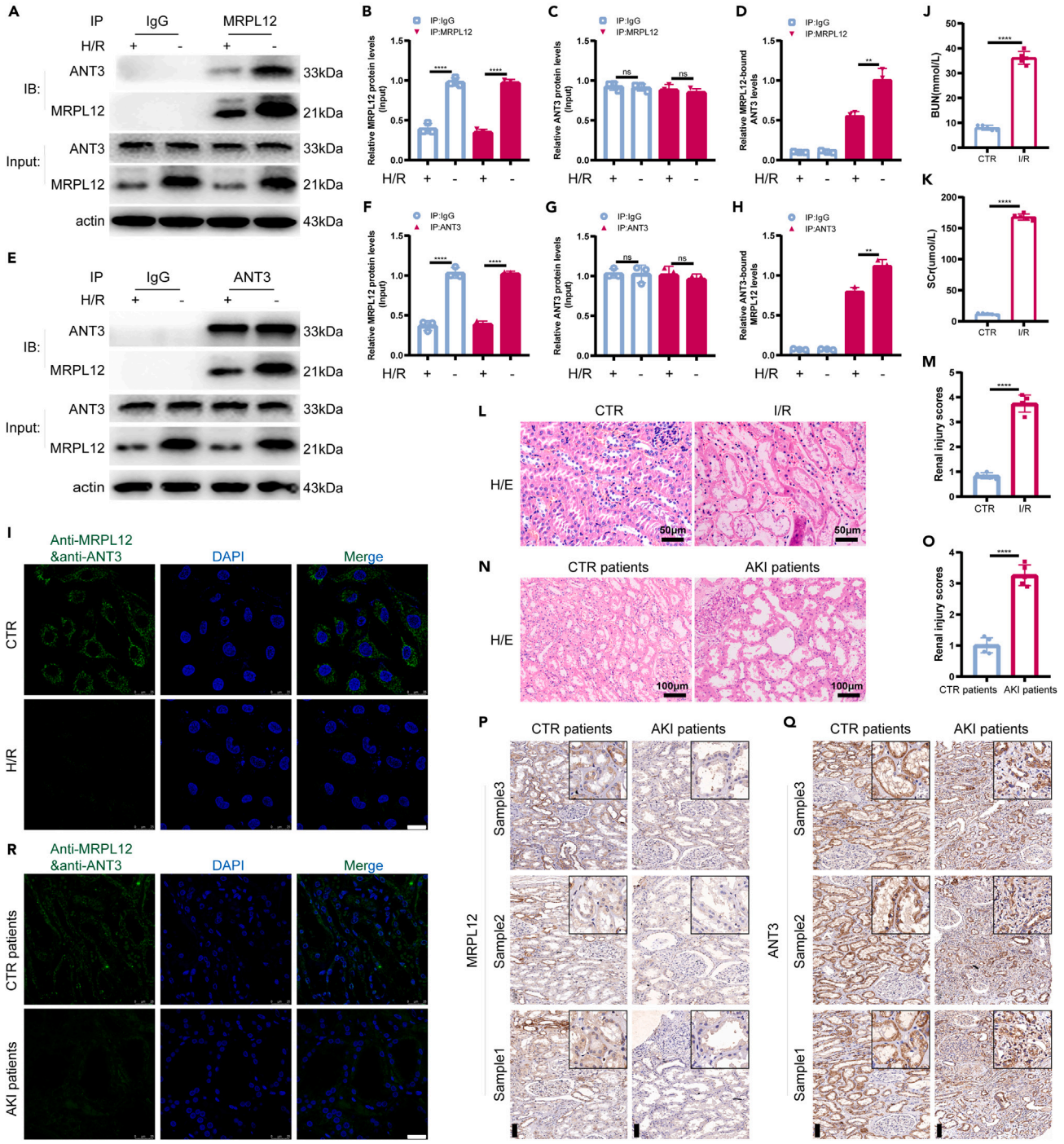

Figure 5. The MRPL12/ANT3 interaction is diminished in I/R-injured kidneys and H/R-treated HK-2 cells

(A and E) Coimmunoprecipitation with endogenous proteins indicated that MRPL12 physically interacted with ANT3. HK-2 cells were treated with H/R or left untreated. Cell lysates were immunoprecipitated with normal IgG, MRPL12 (A), or ANT3 (E) antibody. The immunoprecipitates were immunoblotted (IB) with MRPL12 and ANT3 antibodies. The interaction between MRPL12 and ANT3 was diminished by H/R treatment.

(B, C, F, and G) Quantifications of MRPL12 (B, F) and ANT3 (C, G) expression as shown in A and E, respectively.

(D and H) Quantifications of ANT3 immunoprecipitated with MRPL12 (D) and of MRPL12 immunoprecipitated with ANT3 (H), as shown in A and E, respectively. The coimmunoprecipitated proteins were normalized to β-actin.

(I) Interaction of MRPL12 and ANT3 in HK-2 cells visualized by the Duolink® proximity ligation assay. Scale bars = 25 μm.

(J and K) Renal function of mice was evaluated by serum creatinine (sCr) and blood urea nitrogen (BUN).

Figure 5. *Continued*

(L–O) HE staining for patients and mice with AKI compared with controls. Scale bars = 50 or 100 μm. Renal tubule injury was quantitatively analyzed. (P and Q) Representative images of immunohistochemical staining for MRPL12 and ANT3 expression in the human renal cortex. Scale bars = 100 μm. (R) Interaction of MRPL12 and ANT3 in the human renal cortex visualized by the Duolink® proximity ligation assay. Scale bars = 25 μm. The independent experiments above were performed at least in triplicate. The differences were analyzed by Student's *t* test. Data are presented as the mean ± SD, **p<0.01, ***p<0.001 and ****p<0.0001.

of them are stably associated with membranes independent of the presence of a nascent chain.[37,38] This suggested that specialized proteins that anchor the mitoribosome to the membrane exist. Steric constraints dictate that such a membrane anchor protein would be localized close to the exit of the polypeptide tunnel to optimally position the mitoribosome for membrane insertion of newly synthesized proteins.[37,38] Our immunoelectron microscopic results demonstrated that MRPL12 exists in the mitochondrial membrane (Figures S2A–S2D), suggesting that MRPL12 is probably a membrane-tethered mitochondrial protein.

Of interest, we found that MRPL12 located in the mitochondrial membrane was not limited to facilitating the cotranslational membrane insertion of the synthesized proteins but was directly involved in the crucial process of cell apoptosis by manipulating MPTP. We demonstrate that MRPL12 plays an essential role in mitochondrial membrane homeostasis.

To be clear, proximal tubule cell apoptosis was quantitatively minor than necrosis *in vivo* AKI models (Figures 5L–5R and S5A–S5C). Because unlike the HK-2 cells, which have high glycolytic capacity, fully differentiated proximal tubule cells are not significantly glycolytic and thus develop complete energetic collapse during the MPT. Although apoptosis phenomenon *in vivo* was not as significant as *in vitro*, it still was seen *in vivo* apoptosis cells that MRPL12 is diminished whereas ANT3 remains unchanged. Moreover, it did not affect the significance of decreased MRPL12/ANT3 interaction leading to increased MPTP sensitivity in AKI.

It has been reported that TDZD-8 blocks GSK3b activity and prevents GSK3b-mediated CypD phosphorylation and the ensuing mitochondrial permeability transition, hence ameliorating NSAID-induced AKI.[22] In addition, inhibition or knockout of CypD protected mice from renal IRI by reducing cell death.[39] Moreover, knockdown of SLC25A5 (ANT2, a component of the MPTP) also markedly reduced APOL1 RV-induced cell death.[21] Our study is the first to report that MRPL12 protects renal tubular epithelial cells from apoptosis in AKI by interacting with ANT3, which regulates MPTP opening.

Furthermore, in particular we are interested in the possibility of testing on IRI-sensitive tissue cell lines (e.g., myocardial or endothelial cells). In the future, additional studies will be needed to better understand the effects of MRPL12 on mitochondrial function in the different pathological models driven by IRI. And we could also test various levels of ischemia and reperfusion damage in animal model by modulating the timing of ischemia and reperfusion injury, and then explore the roles of the MRPL12-ANT3 axis respectively.

In summary, our study suggests that MRPL12 can serve as a potential therapeutic target for AKI by maintaining the proper function of MPTP.

Limitations of the study

The current study has two limitations. First, although we investigated the regulatory mechanism of MRPL12 on MPTP in AKI, we analyzed only one crucial cell phenotype, apoptosis. In fact, more than one pathological phenotype of renal tubular epithelial cells was supposed to be MPTP-related in AKI. Second, we identified the interaction domains through protein truncation experiments, but did not further screen small molecule compounds or peptides as potential targeted drugs based on the interaction domains. Further investigation is required in the future.

STAR★METHODS

Detailed methods are provided in the online version of this paper and include the following:

- KEY RESOURCES TABLE
- RESOURCE AVAILABILITY
  - Lead contact
  - Materials availability

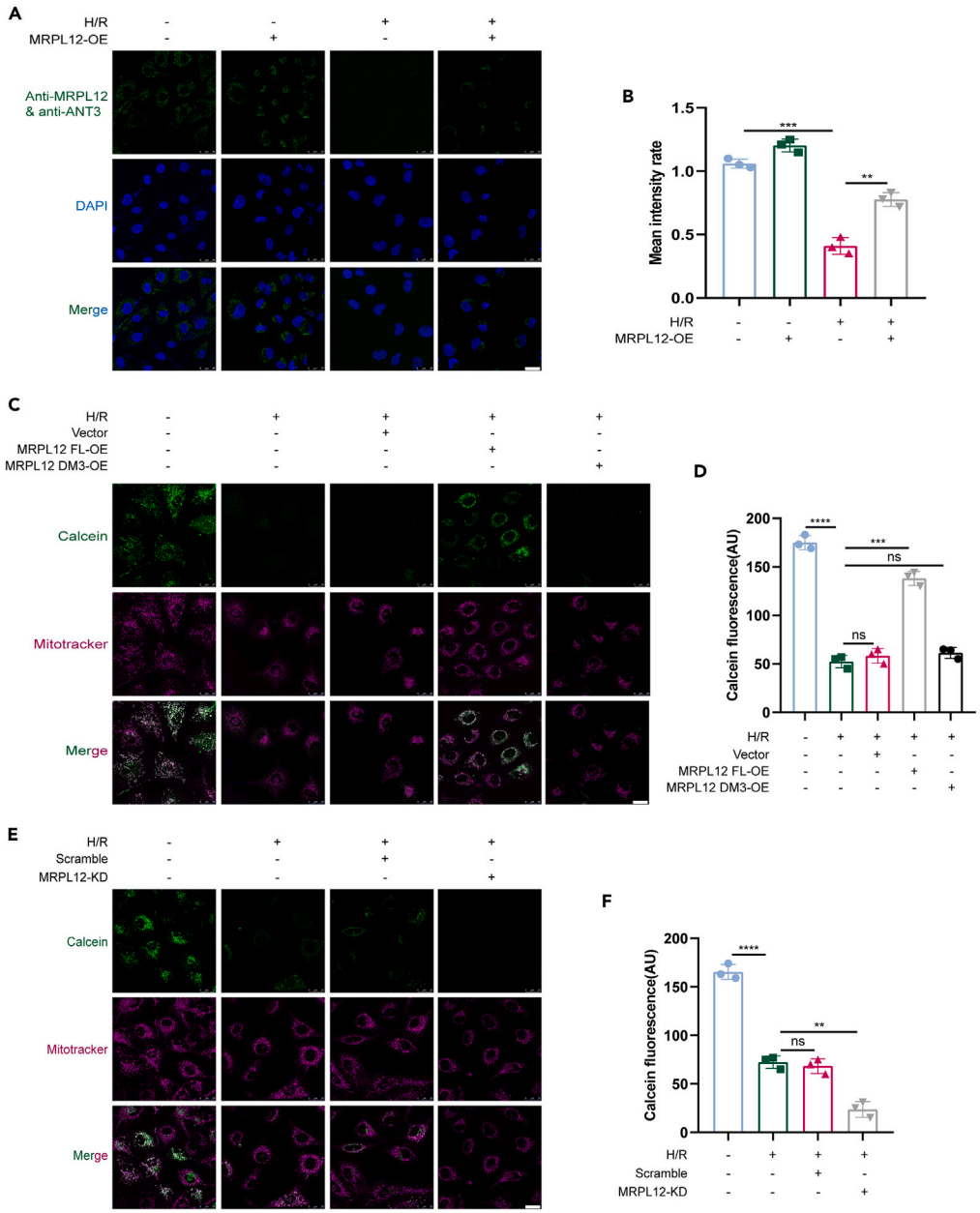

Figure 6. MRPL12 attenuates MPTP opening by interacting with ANT3 under H/R conditions

(A) HK-2 cells transfected with MRPL12 FL-overexpressing plasmid were subjected to H/R treatment, and the interaction of MRPL12 and ANT3 was visualized by a Duolink@ proximity ligation assay. Scale bars = 25 μm.

(B) Mean intensity was calculated by Image J and is shown in the histogram.

(C) HK-2 cells transfected with empty vector, MRPL12 FL-overexpressing plasmid or MRPL12 DM3-overexpressing plasmid were subjected to H/R treatment. The opening of the MPTP in HK-2 cells was detected by a $CoCl_2$-calcein fluorescence quenching assay. Scale bars = 25 μm.

(D) Quantification of calcein fluorescence was performed using Image J and is shown in the histogram.

(E) HK-2 cells transfected with scramble shRNA or MRPL12-silencing shRNA were subjected to H/R treatment. The opening of the MPTP in HK-2 cells was detected by a $CoCl_2$-calcein fluorescence quenching assay. Scale bars = 25 μm.

(F) Quantification of calcein fluorescence was performed using Image J and is shown in the histogram. The independent experiments above were performed in triplicate. The differences were analyzed by Student's *t* test. Data are presented as the mean ± SD, **p<0.01, ***p<0.001 and ****p<0.0001.

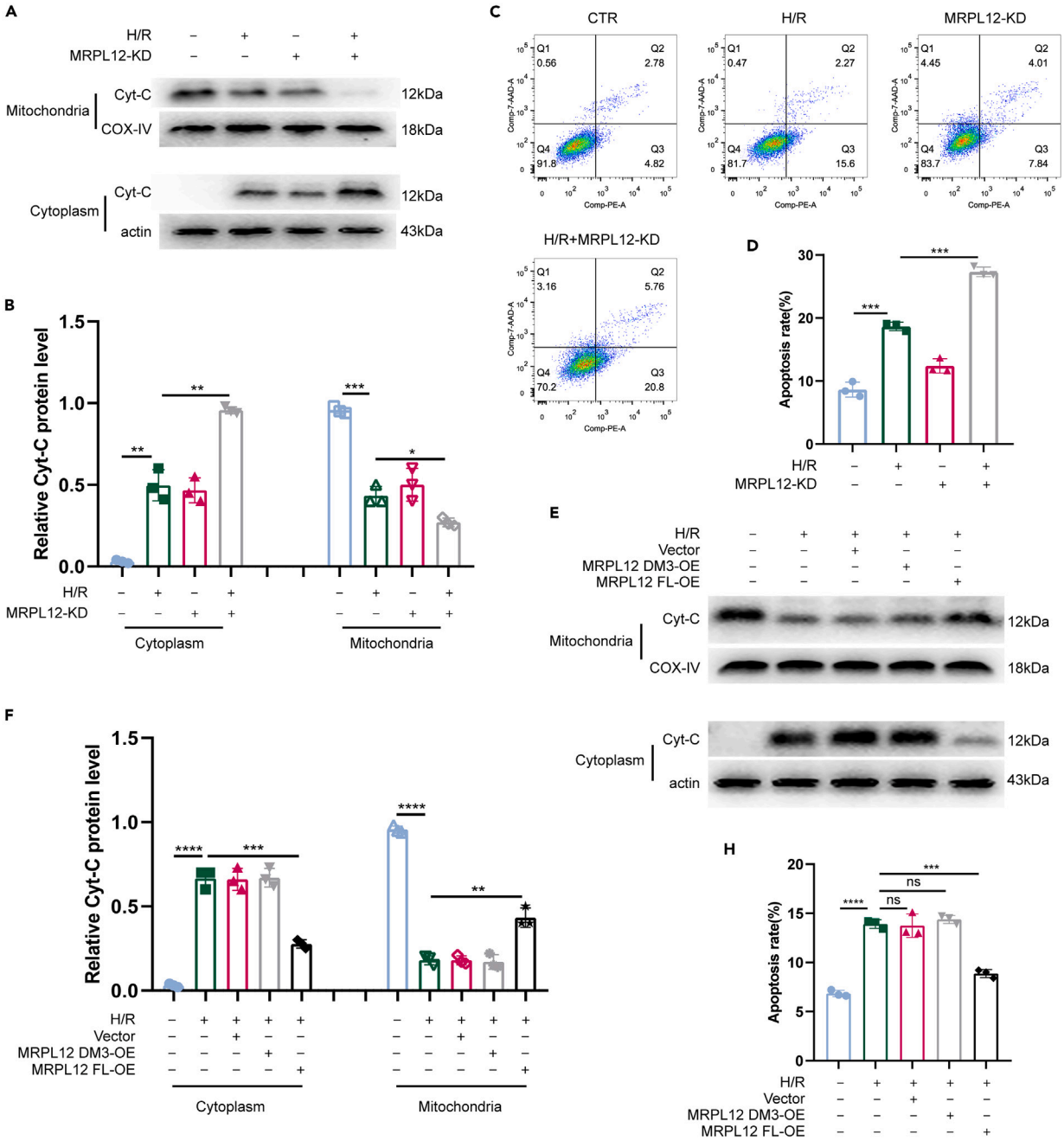
A
H/R
MRPL12-KD
Mitochondria
Cyt-C
COX-IV
12kDa
18kDa
Cytoplasm
Cyt-C
actin
12kDa
43kDa
B
Relative Cyt-C protein level
H/R
MRPL12-KD
Cytoplasm
Mitochondria
C
CTR
H/R
MRPL12-KD
H/R+MRPL12-KD
Comp-7-AAD-A
Comp-PE-A
D
Apoptosis rate(%)
E
Vector
MRPL12 DM3-OE
MRPL12 FL-OE
F
G
H/R+Vector
H/R+MRPL12 DM3-OE
H/R+MRPL12 FL-OE
H
ns

Figure 7. MRPL12 alleviates mitochondria-mediated apoptosis by interacting with ANT3 under H/R conditions

(A and B) The release of cyt-C from the mitochondria to the cytoplasm in HK-2 cells was assessed by Western blot analysis. HK-2 cells transfected with MRPL12-silencing shRNA were subjected to H/R treatment.

(C and D) Apoptosis in HK-2 cells was detected by flow cytometry analysis. HK-2 cells transfected with MRPL12-silencing shRNA were subjected to H/R treatment. The results of flow cytometry analysis were quantified.

(E and F) The release of cyt-C from the mitochondria to the cytoplasm in HK-2 cells was assessed by Western blot analysis. HK-2 cells transfected with empty vector, MRPL12 FL-overexpressing plasmid or MRPL12 DM3-overexpressing plasmid were subjected to H/R treatment.

(G and H) Apoptosis in HK-2 cells was detected by flow cytometry analysis. HK-2 cells transfected with empty vector, MRPL12 FL-overexpressing plasmid or MRPL12 DM3-overexpressing plasmid were subjected to H/R treatment. The results of flow cytometry analysis were quantified. The independent experiments above were performed in triplicate. The differences were analyzed by Student's *t* test. Data are presented as the mean ± SD, *p< 0.05, **p<0.01, ***p<0.001 and ****p<0.0001.

SUPPLEMENTAL INFORMATION

Supplemental information can be found online at https://doi.org/10.1016/j.isci.2023.106656.

ACKNOWLEDGMENTS

We thank all our authors listed in this manuscript, and we also thank Figdraw. This work was supported by the National Natural Science Foundation of China (82271622, 82071569, 82070756, 82102395, 82200049, and 83101639), Shandong Provincial Natural Science Foundation (ZR2021QH083, ZR2019MH003, ZR2021ZD35, ZR202111250039, ZR2022QH349 and ZR2022QH374), Jinan Science and Technology Plan Project (202134046 and 202019064), Jinan Key Laboratory of Medical Sciences Foundation (20211201), Evergreen tree Excellent Young and middle-aged Doctors Training Project of Central Hospital Affiliated to Shandong First Medical University (GDRC2021002).

AUTHOR CONTRIBUTIONS

Investigation, X.J., L.C., and D.S.; Writing – Original Draft, L.C., X.J., and J.S.; Writing – Review and Editing, X.J., Y.W., and Q.W.; Visualization, L.C., D.S., P.S., S.S., and Q.M.; Supervision and Project Administration, Q.W. and Y.L.

DECLARATION OF INTERESTS

All authors declare no conflict of interest.

INCLUSION AND DIVERSITY

We support inclusive, diverse, and equitable conduct of research.

Received: November 28, 2022
Revised: April 4, 2023
Accepted: April 7, 2023
Published: April 14, 2023

REFERENCES

1. Ronco, C., Bellomo, R., and Kellum, J.A. (2019). Acute Kidney Injury (Lancet).

2. Xu, T., Guo, J., Wei, M., Wang, J., Yang, K., Pan, C., Pang, J., Xue, L., Yuan, Q., Xue, M., et al. (2021). Aldehyde dehydrogenase 2 protects against acute kidney injury by regulating autophagy via the Beclin-1 pathway. JCI insight *6*, e138183. https://doi.org/10.1172/jci.insight.138183.

3. Ying, Y., and Padanilam, B.J. (2016). Regulation of necrotic cell death: p53, PARP1 and cyclophilin D-overlapping pathways of regulated necrosis? Cell. Mol. Life Sci. *73*, 2309–2324. https://doi.org/10.1007/s00018-016-2202-5.

4. Zhao, M., Wang, Y., Li, L., Liu, S., Wang, C., Yuan, Y., Yang, G., Chen, Y., Cheng, J., Lu, Y., and Liu, J. (2021). Mitochondrial ROS promote mitochondrial dysfunction and inflammation in ischemic acute kidney injury by disrupting TFAM-mediated mtDNA maintenance. Theranostics *11*, 1845–1863. https://doi.org/10.7150/thno.50905.

5. Duann, P., and Lin, P.H. (2017). Mitochondria damage and kidney disease. Adv. Exp. Med. Biol. *982*, 529–551. https://doi.org/10.1007/978-3-319-55330-6_27.

6. Zuk, A., and Bonventre, J.V. (2016). Acute kidney injury. Annu. Rev. Med. *67*, 293–307. https://doi.org/10.1146/annurev-med-050214-013407.

7. Kers, J., Leemans, J.C., and Linkermann, A. (2016). An overview of pathways of regulated necrosis in acute kidney injury. Semin. Nephrol. *36*, 139–152. https://doi.org/10.1016/j.semnephrol.2016.03.002.

8. Bauer, T.M., and Murphy, E. (2020). Role of mitochondrial calcium and the permeability transition pore in regulating cell death. Circ. Res. *126*, 280–293. https://doi.org/10.1161/circresaha.119.316306.

9. Bround, M.J., Bers, D.M., and Molkentin, J.D. (2020). A 20/20 view of ANT function in mitochondrial biology and necrotic cell death. J. Mol. Cell. Cardiol. *144*, A3–A13. https://doi.org/10.1016/j.yjmcc.2020.05.012.

10. Kwong, J.Q., and Molkentin, J.D. (2015). Physiological and pathological roles of the mitochondrial permeability transition pore in the heart. Cell Metabol. *21*, 206–214. https://doi.org/10.1016/j.cmet.2014.12.001.

11. Brenner, C., Subramaniam, K., Pertuiset, C., and Pervaiz, S. (2011). Adenine nucleotide translocase family: four isoforms for apoptosis modulation in cancer. Oncogene *30*, 883–895. https://doi.org/10.1038/onc.2010.501.

12. Stepien, G., Torroni, A., Chung, A.B., Hodge, J.A., and Wallace, D.C. (1992). Differential expression of adenine nucleotide translocator isoforms in mammalian tissues and during muscle cell differentiation. J. Biol. Chem. *267*, 14592–14597.

13. Li, K., Warner, C.K., Hodge, J.A., Minoshima, S., Kudoh, J., Fukuyama, R., Maekawa, M., Shimizu, Y., Shimizu, N., and Wallace, D.C. (1989). A human muscle adenine nucleotide translocator gene has four exons, is located on chromosome 4, and is differentially expressed. J. Biol. Chem. *264*, 13998–14004.

14. Giraud, S., Bonod-Bidaud, C., Wesolowski-Louvel, M., and Stepien, G. (1998). Expression of human ANT2 gene in highly proliferative cells: GRBOX, a new transcriptional element, is involved in the regulation of glycolytic ATP import into mitochondria. J. Mol. Biol. *281*, 409–418. https://doi.org/10.1006/jmbi.1998.1955.

15. Schiebel, K., Weiss, B., Wöhrle, D., and Rappold, G. (1993). A human pseudoautosomal gene, ADP/ATP translocase, escapes X-inactivation whereas a homologue on Xq is subject to X-inactivation. Nat. Genet. *3*, 82–87. https://doi.org/10.1038/ng0193-82.

16. Dolce, V., Scarcia, P., Iacopetta, D., and Palmieri, F. (2005). A fourth ADP/ATP carrier isoform in man: identification, bacterial expression, functional characterization and tissue distribution. FEBS Lett. *579*, 633–637. https://doi.org/10.1016/j.febslet.2004.12.034.

17. Ruprecht, J.J., and Kunji, E.R.S. (2020). The SLC25 mitochondrial carrier family: structure and mechanism. Trends Biochem. Sci. *45*, 244–258. https://doi.org/10.1016/j.tibs.2019.11.001.

18. Ruprecht, J.J., King, M.S., Zögg, T., Aleksandrova, A.A., Pardon, E., Crichton, P.G., Steyaert, J., and Kunji, E.R.S. (2019). The molecular mechanism of transport by the mitochondrial ADP/ATP carrier. Cell *176*, 435–447.e15. https://doi.org/10.1016/j.cell.2018.11.025.

19. Pebay-Peyroula, E., Dahout-Gonzalez, C., Kahn, R., Trézéguet, V., Lauquin, G.J.M., and Brandolin, G. (2003). Structure of mitochondrial ADP/ATP carrier in complex with carboxyatractyloside. Nature *426*, 39–44. https://doi.org/10.1038/nature02056.

20. Namba, T., Dóczi, J., Pinson, A., Xing, L., Kalebic, N., Wilsch-Bräuninger, M., Long, K.R., Vaid, S., Lauer, J., Bogdanova, A., et al. (2020). Human-specific ARHGAP11B acts in mitochondria to expand neocortical progenitors by glutaminolysis. Neuron *105*, 867–881.e9. https://doi.org/10.1016/j.neuron.2019.11.027.

21. Shah, S.S., Lannon, H., Dias, L., Zhang, J.Y., Alper, S.L., Pollak, M.R., and Friedman, D.J. (2019). APOL1 kidney risk variants induce cell death via mitochondrial translocation and opening of the mitochondrial permeability transition pore. J. Am. Soc. Nephrol. *30*, 2355–2368. https://doi.org/10.1681/ASN.2019020114.

22. Bao, H., Ge, Y., Zhuang, S., Dworkin, L.D., Liu, Z., and Gong, R. (2012). Inhibition of glycogen synthase kinase-3β prevents NSAID-induced acute kidney injury. Kidney Int. *81*, 662–673. https://doi.org/10.1038/ki.2011.443.

23. Briston, T., Selwood, D.L., Szabadkai, G., and Duchen, M.R. (2019). Mitochondrial permeability transition: a molecular lesion with multiple drug targets. Trends Pharmacol. Sci. *40*, 50–70. https://doi.org/10.1016/j.tips.2018.11.004.

24. Rötig, A. (2011). Human diseases with impaired mitochondrial protein synthesis. Biochim. Biophys. Acta *1807*, 1198–1205. https://doi.org/10.1016/j.bbabio.2011.06.010.

25. Smits, P., Saada, A., Wortmann, S.B., Heister, A.J., Brink, M., Pfundt, R., Miller, C., Haas, D., Hantschmann, R., Rodenburg, R.J.T., et al. (2011). Mutation in mitochondrial ribosomal protein MRPS22 leads to Cornelia de Lange-like phenotype, brain abnormalities and hypertrophic cardiomyopathy. Eur. J. Hum. Genet. *19*, 394–399. https://doi.org/10.1038/ejhg.2010.214.

26. Saada, A., Shaag, A., Arnon, S., Dolfin, T., Miller, C., Fuchs-Telem, D., Lombes, A., and Elpeleg, O. (2007). Antenatal mitochondrial disease caused by mitochondrial ribosomal protein (MRPS22) mutation. J. Med. Genet. *44*, 784–786. https://doi.org/10.1136/jmg.2007.053116.

27. Sotgia, F., Whitaker-Menezes, D., Martinez-Outschoorn, U.E., Salem, A.F., Tsirigos, A., Lamb, R., Sneddon, S., Hulit, J., Howell, A., and Lisanti, M.P. (2012). Mitochondria "fuel" breast cancer metabolism: fifteen markers of mitochondrial biogenesis label epithelial cancer cells, but are excluded from adjacent stromal cells. Cell Cycle *11*, 4390–4401. https://doi.org/10.4161/cc.22777.

28. Xie, J., Talaska, A.E., and Schacht, J. (2011). New developments in aminoglycoside therapy and ototoxicity. Hear. Res. *281*, 28–37. https://doi.org/10.1016/j.heares.2011.05.008.

29. Nouws, J., Goswami, A.V., Bestwick, M., McCann, B.J., Surovtseva, Y.V., and Shadel, G.S. (2016). Mitochondrial ribosomal protein L12 is required for POLRMT stability and exists as two forms generated by alternative proteolysis during import. J. Biol. Chem. *291*,

989–997. https://doi.org/10.1074/jbc.M115.689299.

30. Surovtseva, Y.V., Shutt, T.E., Cotney, J., Cimen, H., Chen, S.Y., Koc, E.C., and Shadel, G.S. (2011). Mitochondrial ribosomal protein L12 selectively associates with human mitochondrial RNA polymerase to activate transcription. Proc. Natl. Acad. Sci. USA *108*, 17921–17926. https://doi.org/10.1073/pnas.1108852108.

31. Yang, Y., Li, C., Gu, X., Zhen, J., Zhu, S., Lv, T., Wan, Q., and Liu, Y. (2021). ING2 controls mitochondrial respiration via modulating MRPL12 ubiquitination in renal tubular epithelial cells. Front. Cell Dev. Biol. *9*, 700195. https://doi.org/10.3389/fcell.2021.700195.

32. Ma, Y., Zhu, S., Lv, T., Gu, X., Feng, H., Zhen, J., Xin, W., and Wan, Q. (2020). SQSTM1/p62 controls mtDNA expression and participates in mitochondrial energetic adaption via MRPL12. iScience *23*, 101428. https://doi.org/10.1016/j.isci.2020.101428.

33. Han, M.J., Cimen, H., Miller-Lee, J.L., Koc, H., and Koc, E.C. (2011). Purification of human mitochondrial ribosomal L7/L12 stalk proteins and reconstitution of functional hybrid ribosomes in Escherichia coli. Protein Expr. Purif. *78*, 48–54. https://doi.org/10.1016/j.pep.2011.03.004.

34. Bonora, M., Morganti, C., Morciano, G., Giorgi, C., Wieckowski, M.R., and Pinton, P. (2016). Comprehensive analysis of mitochondrial permeability transition pore activity in living cells using fluorescence-imaging-based techniques. Nat. Protoc. *11*, 1067–1080. https://doi.org/10.1038/nprot.2016.064.

35. Liu, G., Wang, Z.K., Wang, Z.Y., Yang, D.B., Liu, Z.P., and Wang, L. (2016). Mitochondrial permeability transition and its regulatory components are implicated in apoptosis of primary cultures of rat proximal tubular cells exposed to lead. Arch. Toxicol. *90*, 1193–1209. https://doi.org/10.1007/s00204-015-1547-0.

36. Tábara, L.C., Poveda, J., Martin-Cleary, C., Selgas, R., Ortiz, A., and Sanchez-Niño, M.D. (2014). Mitochondria-targeted therapies for acute kidney injury. Expet Rev. Mol. Med. *16*, e13. https://doi.org/10.1017/erm.2014.14.

37. Itoh, Y., Andréll, J., Choi, A., Richter, U., Maiti, P., Best, R.B., Barrientos, A., Battersby, B.J., and Amunts, A. (2021). Mechanism of membrane-tethered mitochondrial protein synthesis. Science (New York, N.Y.) *371*, 846–849. https://doi.org/10.1126/science.abe0763.

38. Greber, B.J., and Ban, N. (2016). Structure and function of the mitochondrial ribosome. Annu. Rev. Biochem. *85*, 103–132. https://doi.org/10.1146/annurev-biochem-060815-014343.

39. Pefanis, A., Ierino, F.L., Murphy, J.M., and Cowan, P.J. (2019). Regulated necrosis in kidney ischemia-reperfusion injury. Kidney Int. *96*, 291–301. https://doi.org/10.1016/j.kint.2019.02.009.

40. Li, X., Liao, J., Su, X., Li, W., Bi, Z., Wang, J., Su, Q., Huang, H., Wei, Y., Gao, Y., et al. (2020). Human urine-derived stem cells protect against renal ischemia/reperfusion injury in a rat model via exosomal miR-146a-5p which targets IRAK1. Theranostics *10*, 9561–9578. https://doi.org/10.7150/thno.42153.

41. Lv, T., Lu, Y., Liu, Y., Feng, H., Li, C., Sheng, W., Cui, Z., Zhu, S., Gu, X., Yang, Z., and Wan, Q. (2021). General control of amino acid synthesis 5-like 1-mediated acetylation of manganese superoxide dismutase regulates oxidative stress in diabetic kidney disease. Oxid. Med. Cell. Longev. *2021*, 6691226. https://doi.org/10.1155/2021/6691226.

STAR★METHODS

KEY RESOURCES TABLE

REAGENT or RESOURCE	SOURCE	IDENTIFIER
Antibodies		
Rabbit polyclonal anti-MRPL12	Proteintech	Cat#14795-1-AP; RRID: AB_2250805
Mouse monoclonal anti-MRPL12	Abnova	Cat#H00006182-M01; RRID: AB_425660
Rabbit polyclonal anti-ANT3	Proteintech	Cat#14841-1-AP; RRID: AB_2190371
Rabbit polyclonal anti-ANT1/2	Proteintech	Cat#15997-1-AP; RRID: AB_2190199
Rabbit polyclonal anti-MRPL11	Proteintech	Cat#15543-1-AP; RRID: AB_2297856
Mouse monoclonal anti-MRPL11	OriGene	Cat#TA505301; RRID: AB_2622984
Mouse monoclonal anti-β-actin	Proteintech	Cat#66009-1-Ig; RRID: AB_2687938
Rabbit polyclonal anti-FLAG	Cell Signaling Technology	Cat#14793S; RRID: AB_2572291
Rabbit polyclonal anti-HA	Cell Signaling Technology	Cat#3724S; RRID: AB_1549585
Mouse monoclonal anti-cytochrome C	Proteintech	Cat#66264-1-Ig; RRID: AB_2716798
Rabbit polyclonal anti-COX IV	Proteintech	Cat#11242-1-AP; RRID: AB_2085278
Rabbit polyclonal anti-ND1	Proteintech	Cat#19703-1-AP; RRID: AB_10637853
Rabbit polyclonal anti-ND5	Proteintech	Cat#55410-1-AP; RRID: AB_2881324
Rabbit polyclonal anti-COX II	Proteintech	Cat#55070-1-AP; RRID: AB_10859832
Rabbit polyclonal anti-CYTB	Proteintech	Cat#55090-1-AP; RRID: AB_2881266
Rabbit polyclonal anti-ATP6V1A	Proteintech	Cat#17115-1-AP; RRID: AB_2290195
Rabbit IgG isotype control	Cell Signaling Technology	Cat#3900, RRID: AB_1550038
Goat anti-Rabbit IgG (H + L) Secondary Antibody	Invitrogen	Cat#65–6120; RRID: AB_2533967
Goat anti-Mouse IgG (H + L) Secondary Antibody	Invitrogen	Cat#31430, RRID: AB_228307
Bacterial and virus strains		
LV16-homo-MRPL12-shRNA2 (target sequence:5′-TCAACGAGCTCCTGAAGAAA-3′)	GenePharma	N/A
Biological samples		
Renal biopsy specimens	Cheeloo College of Medicine, Shandong University	N/A
Control samples from healthy kidney poles	Cheeloo College of Medicine, Shandong University	N/A
Chemicals, peptides, and recombinant proteins		
Atractyloside potassium salt	Selleck Chemicals	Cat#S3264; CAS: 102130-43-8
Bongkrekic acid	Enzo Life Science	Cat#BML-CM113; CAS: 1177154-51-6
Critical commercial assays		
Duolink™*In Situ* PLA kit	Sigma	Cat#DUO92101
Image-IT live mitochondrial transition pore assay kit	Thermo Fisher Scientific	Cat#I35103
Cell Mitochondria Isolation Kit	Beyotime	Cat#C3601
PE Annexin V Apoptosis Detection Kit	BD Biosciences	Cat#559763
Pierce™ IP Lysis Buffer	Thermo Scientific™	Cat#87788
Protein A/G Magnetic Beads	Bimake	Cat#B23202
Deposited data		
Original western blotData	Mendeley Data	https://doi.org/10.17632/w78ft82ndv.1
Mass spectrometryData	Mendeley Data	https://doi.org/10.17632/fxw9y6m6v9.1

(*Continued on next page*)

Continued

REAGENT or RESOURCE	SOURCE	IDENTIFIER
Experimental models: Cell lines		
Human kidney cortex/proximal tubule cells (HK-2)	ATCC	Cat#CRL-2190; RRID: CVCL_0302
HEK293T cells	ATCC	Cat#CRL-3216; RRID: CVCL_0063
Experimental models: Organisms/strains		
C57BL/6J mice	Vital River Laboratory	Cat#NR00206
MRPL12-flox/flox mice	Shanghai Model Organisms Center	N/A
Ksp1.3-Cre mice	Jackson Laboratory	RRID: IMSR_JAX:012237
TEC-MRPL12$^{-/-}$ mice	This paper	N/A
Oligonucleotides		
Hs-ANT3-siRNA#1(target sequence:5′-GTCGACTGTTGGAGGAAGA-3′)	RIBOBIO	N/A
Hs-ANT3-siRNA#2(target sequence:5′-GCAACCTTGCCAACGTCAT-3′)	RIBOBIO	N/A
Hs-ANT3-siRNA#3(target sequence:5′-GAGACTGCCTGGTGAAGAT-3′)	RIBOBIO	N/A
Primers for RT-qPCR assay, see Table S3	BioSune	N/A
Recombinant DNA		
pcDNA3.1(+)-ANT3-FLAG	BioSune	Cat#G0197700-2
pcDNA3.1(+)-MRPL12(FL)-HA	BioSune	Cat#G0197700-3
pcDNA3.1(+)-MRPL12(DM1)-HA	BioSune	Cat#G0213760-1
pcDNA3.1(+)-MRPL12(DM2)-HA	BioSune	Cat#G0202307-1
pcDNA3.1(+)-MRPL12(DM3)-HA	BioSune	Cat#G0213760-2
pcDNA3.1(+)-MRPL12(DM4)-HA	BioSune	Cat#G0197700-1
Software and algorithms		
ImageJ	NIH	https://imagej.nih.gov/ij/
FlowJo	BD	RRID: SCR_008520
GraphPad Prism 8.0	GraphPad Software	RRID: SCR_002798
UniProtKB	The UniProt consortium	https://www.uniprot.org/
SWISS-MODEL	The SIB Swiss Institute of Bioinformatics	https://swissmodel.expasy.org/
ZDOCK	HOME for Researchers	https://www.dockeasy.cn/DockProtein

RESOURCE AVAILABILITY

Lead contact

Further information and requests for resources and reagents should be directed to and will be fulfilled by the lead contact, Qiang Wan (wanqiang@sdu.edu.cn).

Materials availability

All unique reagents generated in this study are available from the lead contact with a completed Materials Transfer Agreement.

Data and code availability

- Data: Mass spectrometrydata and Original western blot images have been deposited at Mendeley and are publicly available as of the date of publication. The DOI is listed in the key resources table. Microscopy data reported in this paper will be shared by the lead contact upon request.
- Code: This paper does not report original code.

- All other requests: Any additional information required to reanalyze the data reported in this paper is available from the lead contact upon request.

EXPERIMENTAL MODEL AND SUBJECT DETAILS

Human kidney tissues

Renal biopsy specimens from 5 male patients (The age was 30, 33, 45, 53 and 70 years, respectively) with diagnosis of acute tubular injury (ATI) were obtained from Cheeloo College of Medicine, Shandong University. All patients developed stage 3 AKI. AKI staging is based on kidney disease improving global outcomes (KDIGO) guidelines (Table S2). Baseline renal parameters are similar between AKI and control group. Control samples were taken from healthy kidney poles of 5 male individuals (The age was 30, 33, 45, 53 and 70 years, respectively) who underwent cancer nephrectomy without other renal diseases. All procedures were approved by the Ethics Review Committee of Shandong University (ECSBMSSDU2018-1-045) and performed in accordance with the principles of the Helsinki Declaration after obtaining informed consent from the patients.

Generation of the TEC-MRPL12$^{-/-}$ mice

Ksp1.3-Cre transgenic mice were purchased from the Jackson Laboratory (ME, USA). MRPL12-flox/flox mice were generated by Shanghai Model Organisms Center, Inc (Shanghai, China). MRPL12-flox/flox mice were bred with Ksp1.3-Cre mice to generate mice with deletion of MRPL12 in renal tubular epithelial cells (TEC-MRPL12$^{-/-}$). The experiments were established in 6 weeksold male TEC-MRPL12$^{-/-}$ mice. All experiments were performed with littermate controls.

Animal model of IRI

The IRI model was established in male adult C57BL/6J mice (7–8 weeks old) purchased from Beijing Vital River Laboratory Animal Technology Co., Ltd (Beijing, China). The mice were fully anesthetized with isoflurane (2%) inhalation and placed on a homeothermic table to maintain core body temperature at 37°C. The right kidney was removed as an internal control, and the left renal artery was then clamped for 30 min to induce ischemia. Mice were killed at 24 h after reperfusion, and the kidneys and blood were collected for further analysis.

All animal projects were approved by the committee of experimental animals of Shandong University, and procedures were carried out in accordance with routine animal-care guidelines. All procedures complied with the Guidelines for the Care and Use of Laboratory Animals. Mice were housed in a specific pathogen-free facility with free access to chow and water and a 12-h day/night cycle.

In vitro model of hypoxia/reoxygenation (H/R)

Human kidney cortex/proximal tubule cells (HK-2) were obtained from the AmericanType Culture Collection (ATCC, MD, USA, CRL-2190, RRID: CVCL_0302). HK-2 is a proximal tubular cell line derived from normal adult male kidney, which proved to be a tool for the study of proximal tubular cell physiology/pathophysiology and mechanisms of cell injury and repair. HK-2 cells were cultured in DMEM (Gibco, CA, USA) supplemented with 10% FBS, 100 U/ml penicillin, and 100 μg/mL streptomycin. For all culture conditions, the cells were incubated in a humidified incubator containing 5% CO_2 at 37°C. The H/R treatment was optimized according to previously described methods.[40] H/R injury was induced in HK-2 cells by incubation in glucose- and serum-free medium in a 1% O_2 environment for 24 h followed by reoxygenation with normal O_2 and medium for 6 h.

METHOD DETAILS

Assessment of renal function and renal pathology

sCr and BUN levels were evaluated as previously described.[32] Acute tubular injury was assessed using semi-quantitative measurements according to hematoxylin-eosin (HE) staining. Two pathologists blinded to this study analyzed the extent of kidney damage in histopathological sections. Histological scoring encompassed grading of tubular necrosis, loss of brush border, cast formation, and tubular dilatation in 10 randomly chosen nonoverlapping fields. The renal injury degree was classified as follows: 0 (nil), 1 (<25%), 2 (25–50%), 3 (50–75%), and 4 (>75% of tubules).

Immunohistochemistry

The sections were baked in a 60°C oven for 2 h and then dewaxed with gradient ethanol. For antigen retrieval, tissue sections were placed in sodium citrate buffer (Servicebio Technology, Wuhan, China) and boiled for 18 min. Then, a PV-9000 kit (ZSGB-BIO, Beijing, China) was used according to the manufacturer's instructions. The tissue sections were incubated with primary antibodies overnight at 4°C. Finally, DAB staining, hematoxylin redyeing and hydrochloric acid alcohol differentiation were performed. The images were captured with an Pannoramic Viewer (3DHISTECH, RRID: SCR_014424).

Cell transfection

si-ANT3 was commercially constructed by RiboBio (Guangzhou, China), and si-CTR (negative control) was used as the control. pcDNA3.1-ANT3-FLAG was constructed by BioSune (Shanghai, China), and an empty pcDNA 3.1 vector was used as the control. The cells were transfected with siRNA using a riboFECTTM CP Transfection kit (Ribobio, China) or overexpression plasmid using Lipofectamine 3000 (Invitrogen, USA) according to the manufacturer's instructions. MRPL12-shRNA retrovirus was purchased from GenePharma (Shanghai, China). One plasmid with full-length MRPL12 (FL) and four plasmids with MRPL12 deletion mutants (DMs) were constructed by BioSune (Shanghai, China). Human embryonic kidney 293T (HEK293T) cells (ATCC, CRL-3216, RRID: CVCL_0063) were cotransfected with ANT3-FLAG and MRPL12 FL-HA or various MRPL12 DMs-HA. Key resources table describes the relevant sequences of siRNA, short hairpin RNAs and recombinant DNA.

Quantitative real-time PCR (qRT–PCR)

qRT–PCR was performed as previously described.[32] Briefly, qRT-PCR was performed as following: 95°C for 30s to denaturation, then 40 cycles of 95°C for 5 s, followed by 60°C for 30s to PCR, 95°C for 5s and 60°C for 1 min, followed by 95°C to melt, finally 50°C for 30s to cool down. The sequence information of the primers are presented in key resources table.

Western blot analysis

Western blot analysis was performed as previously described.[41] Proteins were extracted from cells or kidney tissues by using RIPA buffer supplemented with 1% protease and phosphatase inhibitor cocktail. The protein concentration was measured using a bicinchoninic acid (BCA) reagent (Beyotime Biotechnology, Cat# P0012). After dilution in 4× SDS–PAGE loading buffer and denaturation at 98°C for 10 min, the samples were separated by SDS–PAGE and subsequently transferred to PVDF membranes. The membranes were blocked with 5% skimmed milk and then incubated with primary antibody. Then, the membranes were incubated with the corresponding secondary antibody (HRP-tagged) and detected by enhanced chemiluminescence reagents (Tanon, Shanghai, China). Quantitative analysis was performed using ImageJ (RRID: SCR_003070) software.

Mass spectrometry

HK-2 cells were lysed in Pierce IP Lysis Buffer containing protease and phosphatase inhibitor cocktail. Lysates were incubated overnight with anti-MRPL12 rabbit polyclonal antibody crosslinked Protein A/G Magnetic Beads. The beads were washed three times with washing buffer (20% Pierce IP Lysis Buffer), and the proteins were heated to 98°C in 4× loading buffer. Samples were separated on a 12% SDS–PAGE gel. After gel staining with Coomassie bright blue (Sigma, Cat# B8522), the gel was cut into several small bands, and the gel fragments were sent for protein identification by liquid chromatography with tandem mass spectrometry (LC–MS/MS). Proteome Discoverer 2.2 (RRID:SCR_014477) software was used to further filter the raw results. The identified protein list was generated by performing Gene Ontology (RRID: SCR_002811)/KEGG (RRID: SCR_012773) enrichment analysis followed by UniProtKB (RRID: SCR_004426) processing.

Coimmunoprecipitation

For coimmunoprecipitation experiments, cells were lysed in Pierce IP Lysis Buffer (Thermo Scientific, Cat# 87788) containing protease and phosphatase inhibitor cocktail for 40 min on ice and then centrifuged at 12,000×g for 10 min to remove debris. Lysates were incubated with the Protein A/G Magnetic Beads (Bimake, Cat# B23202)-Antibody complex for 10hat 4°C. After washing three times in washing buffer (20% Pierce IP Lysis Buffer), the samples were heated to 98°C in 4× SDS–PAGE loading buffer for 10 min and then immunoblotted as described above.

In situ proximity ligation assay

HK-2 cells were fixed in 4% paraformaldehyde and permeabilized in 0.5% Triton X-100. The proximity ligation assay was carried out according to the manufacturer's instructions of the Duolink *In Situ* PLA kit (Sigma, Cat# DUO92101). The signal was visualized using a Leica SP8 confocal microscope (Leica Microsystems, RRID: SCR_008960) and analyzed by ImageJ (RRID: SCR_003070) software.

Live cell imaging

MPTP opening was assessed using the Image-IT live mitochondrial transition pore assay kit (Thermo Fisher Scientific, Cat# I35103). Briefly, cells were stained with 1 mM calcein acetoxymethyl ester (calcein-AM), 100 nM MitoTracker Red CMXRos, and 10 mM $CoCl_2$ for 30min at 37°C protected from light. Then, the cells were mounted in warm buffer for viewing. All images were acquired with the Leica SP8 confocal system (Leica Microsystems, RRID: SCR_008960).

Cytosolic cytochrome *C* release

Mitochondria were isolated using a Cell Mitochondria Isolation Kit (Beyotime, Shanghai, China) according to the manufacturer's instructions. Cytochrome *c* release into the cytosolic fraction for each condition was assessed by Western blot analysis.

Flow cytometry apoptosis assay

Detection of HK-2 cell apoptosis was performed using a PE Annexin V Apoptosis Detection Kit I (BD Biosciences, Cat# 559763) in accordance with the manufacturer's instructions. In brief, cells were harvested after trypsin digestion, centrifuged, and washed with Annexin V binding buffer three times. Then, the cells were stained with PE Annexin V and 7-AAD at room temperature for 15 min and analyzed by flow cytometry (BD LSRFortessa, RRID: SCR_019600). Flow cytometry data were analyzed using FlowJo (RRID:SCR_008520) software.

Transmission electron microscopy

Kidneys were dissected and rapidly prefixed with a 3% glutaraldehyde, then the tissue was postfixed in 1% osmium tetroxide, dehydrated in series acetone, infiltrated in Epox 812 for a longer, and embedded. The semithin sections were stained with methylene blue and ultrathin sections were cut with diamond knife, stained with uranyl acetate and lead citrate. Sections were examined with electron microscopy (JEOL, JEM-1400-FLASH, RRID:SCR_020179).

Immunoelectron microscopy

HK-2 cells were grown and cultured with no treatment. For immunoelectron microscopy, cells were first fixed with 2% paraformaldehyde and 0.3% glutaraldehyde in PBS buffer (pH 7.4) at 37°C for 2 h, dehydrated in a graded acetone series and embedded in resin. Ultrathin sections (60–80 nm) were mounted on nickel grids, incubated with 1% BSA/PBS and incubated overnight at 4°C with anti-MRPL12 antibody in 1% BSA/PBS, washed five times for 5 min in 0.5% BSA/PBS and then labeled for 2 h with 10 nm goat anti-rabbit for MRPL12–gold-conjugated particles in 1% BSA/PBS. The grids were finally washed, stained and dried at room temperature. The samples were visualized by electron microscopy (JEOL, JEM-1400FLASH, RRID:SCR_020179).

Molecular docking

The sequences of MRPL12 and ANT3 were searched in the UniProtKB (RRID: SCR_004426). Then, the tertiary structures of them were built using SWISS-MODEL (RRID: SCR_018123). The PDB format of the protein structure was downloaded from the SWISS-MODEL. ZDOCK (RRID: SCR_022518) was used to identify the interaction between MRPL12 and ANT3.

QUANTIFICATION AND STATISTICAL ANALYSIS

Statistical data are expressed as the mean ± SD. All experiments were performed at least three times, and statistical analysis of all data was performed by GraphPad Prism 8.0 (RRID: SCR_002798). Student's *t* test was used for two-group comparisons; one-way ANOVA was used for multiple-group comparisons. Differences with $p < 0.05$ were considered statistically significant. *$p < 0.05$, **$p < 0.01$, ***$p < 0.001$, and****$p < 0.0001$.